JOURNAL OF MATERIALS SCIENCE 31 (1996) 633–641

Microstructural characterization of SiC/Al and FP/Al metal matrix composites subjected to dynamic loadings

M. NANDURI, A. SHUKLA
Dynamic Photomechanics Laboratory, Department of Mechanical Engineering and Applied Mechanics, University of Rhode Island, Kingston, RI 02881, USA

The Split Hopkinson Pressure Bar technique was used to study the dynamic response of silicon carbide particle- and whisker-reinforced aluminium (SiC/Al-P and SiC/Al-W) and continuous Fibre FP-reinforced aluminium (FP/Al), metal matrix composites, subjected to high strain rates in the range of 300–3200 s^{-1}. The response of these composites was characterized by macroscopic and microscopic observations. Experiments on SiC/Al-W and FP/Al were conducted with the whiskers/fibres oriented in the axial, as well as, in the transverse direction with respect to the loading direction. It was observed that for the silicon carbide-reinforced metal matrix composites, the dynamic flow stress values were consistently higher than the static/quasi-static values. Experiments conducted on FP/Al with the fibres oriented transversely to the loading direction, revealed failure stress values considerably lower than the static/quasi-static values. This anomalous behaviour was attributed to the predominantly shear mode failure of the material. Microscopic observations using optical and scanning electron microscopy corroborate the macroscopically observed behaviour.

1. Introduction

The Split Hopkinson Pressure Bar (SHPB) is a well-established experimental technique in the field of dynamic testing. It has been used to study the dynamic behaviour of a wide variety of materials ranging from ductile and brittle metals to ceramics. The Split Hopkinson Pressure Bar is so called due to the pioneering work of Hopkinson and Hopkinson [1–3], who used a single-bar configuration, and the subsequent contribution by Kolsky [4], who "split" the single bar and derived simple relations relating the strains in the bars to the stresses and strains in the specimen sandwiched between the two bars. The Split Hopkinson Pressure Bar is also referred to as the Kolsky bar. Initially, the SHPB technique was used only in the compression mode. Harding *et al.* [5], and later Lindholm and Yeakley [6] modified the SHPB for use in tension mode. Hauser *et al.* [7] used strain gauges to measure surface displacements on the elastic bars, a procedure that has become a standard. Baker and Yew [8] modified the SHPB for dynamic torsion tests. A technique for performing elevated temperature tests was described by Chiddister and Malvern [9]. Lindholm [10] developed an application of the SHPB to dynamic testing of materials, whereby continuous records of strain versus time, strain-rate versus time, stress versus time and stress versus strain may be simultaneously recorded. He also applied the technique to non-metallic materials. Davies and Hunter [11] studied metals and polymeric materials and also derived a relationship between the specimen geometry and its Poisson's ratio to minimize inertia effects inherent in the SHPB system. Follansbee [12] reviewed the development of the SHPB technique, its basic principles, related test equipment and procedures that have been standardized, and the test limitations. Nemat-Nasser *et al.* [13] modified the SHPB for conducting dynamic recovery experiments. Recent studies with the SHPB that included the microscopic aspect were conducted by Ravichandran and Chen [14], da Silva and Ramesh [15] and Hong *et al.* [16].

This paper, describes the experiments conducted on silicon carbide particle-reinforced aluminium, silicon carbide whisker-reinforced aluminium and continuous fibre (FP)-reinforced aluminium using the classical SHPB in compression mode, to identify the micromechanisms involved in the macroscopically apparent dynamic behaviour of these metal matrix composites subjected to uniaxial compression under constant and high strain-rate loading conditions. The primary macroscopic observations are the dynamic flow stress, strain and strain-rate for the material under consideration, obtained from the dynamic stress versus strain, strain versus time and strain-rate versus time plots. Secondary macroscopic observations are the total permanent strain calculated from the initial and final specimen dimensions, the initial and final geometries (readily visible to the naked eye in the case of highly anisotropic materials), and surface topography in the case of fractured specimens. A brief

0022–2461

description of the SHPB technique with the basic theoretical considerations and assumptions, experimental testing and data analysis procedures, mechanical properties and composition of the materials tested, results and discussion, are given.

2. Theoretical background

The SHPB technique yields the highest possible strain rates in a uniaxial compression test under uniform deformation conditions. Fig. 1 is a schematic illustration of the SHPB system. A small cylindrical specimen is sandwiched between the incident and the output bars. A projectile (also called the striker bar) fired from the gas gun strikes the incident bar on the impact end. This generates a compressive pulse equal to twice the length of the striker bar, which travels down the incident bar. Upon reaching the specimen, part of the pulse is reflected back into the incident bar and the rest is transmitted through the output bar. From one-dimensional wave theory, it can be shown that the reflected and the transmitted pulses (which are, in fact, the strain values measured by the strain gauges at stations A and B) are proportional to the strain rate and the stress in the deforming specimen, respectively. The strain–time histories of the incident, reflected and the transmitted pulses recorded by the strain gauges are analysed to yield the stress versus time, strain versus time, strain rate versus time and stress versus strain plots for the specimen material. The specimen can be subjected to a range of strain rates and strain by using various projectile lengths and velocities.

2.1. Basic equations

The classical D'Alembert one-dimensional wave equation is

$$y(x,t) = f(x - c_0 t) + g(x + c_0 t) \tag{1}$$

where f and g represent propagating disturbances. f and g are arbitrary functions of integration determined by the initial conditions of the forcing function of a given problem. f corresponds to a wave propagating in the positive x direction and g corresponds to a wave propagating in the negative x direction. The shape of f and g is maintained without distortion during propagation, which is the fundamental characteristic of the one-dimensional wave equation.

In Fig. 2, the incident, reflected and the transmitted strain waves are represented by ε_i, ε_r, and ε_t, respectively. These strain values are obtained from the strain gauges on the bars. The displacements of the right and left interfaces of the specimen are denoted by u_1, u_2. From one-dimensional rod theory, we have for the wave system in the incident bar

$$\begin{aligned} u &= f(x - c_0 t) + g(x + c_0 t) \\ &= u_i + u_r \\ \varepsilon &= f' + g' = \varepsilon_i + \varepsilon_r \\ \dot{u} &= c_0(-f' + g') = c_0(-\varepsilon_i + \varepsilon_r) \end{aligned} \tag{2}$$

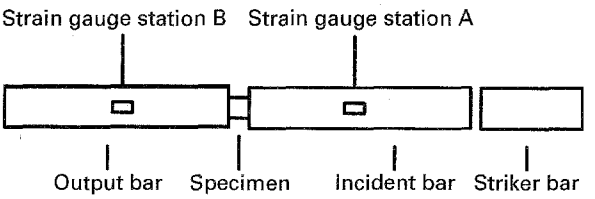

Figure 1 Schematic illustration of the SHPB system.

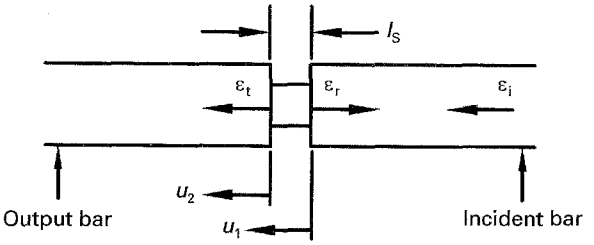

Figure 2 Displacements and strains in the SHPB system.

The displacement u_1, is then given by

$$u_1 = c_0 \int_0^t (-\varepsilon_i + \varepsilon_r) dt \tag{3}$$

The transmitted wave system and the displacement u_2 are given by

$$u = h(x - c_0 t) \tag{4a}$$

$$\varepsilon = h' = \varepsilon_t \tag{4b}$$

$$\dot{u} = -c_0 h' = -c_0 \varepsilon_t \tag{4c}$$

$$u_2 = -c_0 \int_0^t \varepsilon_t dt \tag{4d}$$

The average strain, ε_s, in the specimen is then given by

$$\begin{aligned} \varepsilon_s &= \frac{u_2 - u_1}{l_s} \\ &= \frac{c_0}{l_s} \int_0^t (-\varepsilon_t + \varepsilon_i - \varepsilon_r) dt \end{aligned} \tag{5}$$

where l_s is the original specimen length.

The loads on each face of the specimen are given by

$$P_1 = A_b E_b (\varepsilon_i + \varepsilon_r) \tag{6a}$$

$$P_2 = A_b E_b \varepsilon_t \tag{6b}$$

where A_b is the pressure bar cross-section. The important assumption is now made that wave propagation effects within the short specimen may be neglected, so that $P_1 = P_2$. It follows that $\varepsilon_i + \varepsilon_r = \varepsilon_t$, so that Equation 5 simplifies to

$$\varepsilon_s(t) = \frac{-2c_0}{l_s} \int_0^t (\varepsilon_r) dt \tag{7}$$

The stress in the specimen is given by

$$\sigma_s = \frac{P_1}{A_s} = \frac{P_2}{A_s} \tag{8}$$

where A_s is the specimen instantaneous cross-sectional area.

Average stress in the specimen is

$$\sigma_s = \frac{P_1 + P_2}{2A_s} = \frac{1}{2} E_b \left(\frac{A_b}{A_s}\right)(\varepsilon_i + \varepsilon_r + \varepsilon_t)$$

$$\therefore \sigma_s = E_b \left(\frac{A_b}{A_s}\right) \varepsilon_t \tag{9}$$

For these equations to be valid, two important conditions have to be met.

Condition 1. Wave propagation within the pressure bars must be one-dimensional. In the SHPB system, the strain gauges measure the surface displacements on the bars. These surface displacements are used to represent the axial displacement over the entire cross-sectional area of the pressure bars. The wave propagation effects in the specimen are also neglected.

Condition 2. The specimen must deform uniformly. The uniform deformation of the specimen is opposed by radial and longitudinal inertia of the specimen and by the frictional constraint at the specimen/pressure bar interfaces. Oil-based molybdenum disulphide lubricant is the preferred choice for room-temperature experiments.

The reader is directed to Follansbee [12] for a detailed discussion on these conditions.

3. Experimental procedure

3.1. Experimental equipment

In the present experiment, the incident and output bars were 1.24 m each, in length and 12.7 mm diameter. The l_b/d_b ratio was therefore 97.6 which is ideal to obtain high strain and strain-rate values. The bars are made from VascoMax C-350 steel manufactured by Teledyne Allvac/Vasco. The material is a cobalt strengthened 18% Ni maraging steel with a yield strength of 2675 MPa in the aged condition. The material was received in the solution-annealed state with a yield strength of 1106 MPa and a hardness of 30/35 R_c. The bars were then aged at 950 °F for 3 h. Because the VascoMax alloy C-350 is essentially carbon-free, protective atmospheres are not required while ageing. During the ageing process, the alloy shrinks uniformly and predictably in all dimensions. The shrinkage in this case is 0.001 mm mm^{-1}. Care was taken not to induce any residual and thermal stresses in the bars. The bars were descaled and straightened to close tolerance of 0.127 mm. The aged bars have a 0.2% offset yield strength of 2675 MPa and a hardness of 58/60 R_c.

The design of the specimen is very critical to minimize errors due to inertia and friction. Assuming a maximum strain of 25% within the deforming specimen, the specimen diameter was chosen such that the cross-sectional area of the specimen does not, at any time, exceed the cross sectional area of the pressure bars. Because the diameter of the bars is fixed at 12.7 mm, the diameter of the specimen cannot exceed 10.16 mm. The length of the specimen can then be calculated by using the equation

$$\frac{l_s}{d_s} = \left(\frac{3\nu_s}{4}\right)^{1/2} \tag{10}$$

where l_s, d_s, ν_s are the specimen length, diameter and Poisson's ratio, respectively [11].

The specimen ends were polished and maintained square and parallel to each other. This ensured a good contact with the ends of the pressure bars. All the specimens were fine turned and then polished with increasing grit abrasive paper.

The striker bars were made from the same material as the pressure bars and were aged similarly. The impact ends of all the striker bars were rounded slightly to minimize end effects.

Bearings supported the pressure bars and provided a well-lubricated contact for the bars to be able to translate freely. Self-lubricating-type Oilite bearings were used in the present experiment. The bars passed through these bearings and were allowed to translate freely in the axial direction while being constrained laterally. The clearance between the bearings and the bars was kept between 0.02 and 0.05 mm to allow for the radial expansion of the bars when the stress wave propagated along the bars. A self-compensating linear decelerator was used at the rear end of the output bar. The linear decelerator MC 1201-0 by Ace Controls, retards the output bar to zero velocity at the end of a short stroke. The length of the stroke can be varied according to the impact velocities and the energy of the system. Existing gas gun assembly with a 12.7 mm bore was used to propel the projectiles toward the incident bar. The gun operates on the principle of expansion of a compressible gas such as helium. The maximum operating pressure is 1.38 MPa.

3.2. Data analysis

A pair of strain gauges, diametrically opposite each other (to average out any bending strain), were affixed on each bar. The distance between the strain gauges, on either bar, from the centre of the specimen was exactly the same, to a tolerance of 1 mm. This is very important, because the reflected and transmitted pulses have to reach the strain gauges at the same time. This reduces the error in adjusting the time for the pulses. Terminal pads were attached close to each strain gauge. The strain gauge lead wires were provided with a small loop and soldered to the terminal pad. This protected the leads from breaking when the bars lengthened axially due to tensile waves in the system. The lead wires from the terminal pads on the bars were connected to four Ectron signal conditioners. Each Ectron module acted as a quarter bridge and amplified the strain signal. The amplified signal was fed through a LeCroy data acquisition module (a high-speed analogue to digital converter and recorder capable of sampling the signal at a maximum rate of 50 MHz). A PC-based software called Waveform Catalyst provided the interface to view the recorded signal and store the information on magnetic media. Further data analysis was performed using commercially available plotting software.

It should be noted that the initial portion of the stress versus strain plot for the materials studied, though similar to the elastic portion of a standard stress versus strain plot, does not represent it. The

data from the SHPB technique is only valid in the plastic region because of the inherent errors of the technique such as the time required for the stress wave to "stabilize". The average flow stress obtained from this technique is accurate within an experimental error of $\pm$ 5%.

Typical pulse profiles (raw data), strain versus time and true stress versus true strain plots obtained from the SHPB data analysis are shown in Fig. 3a–c, respectively. The material tested was silicon carbide particle-reinforced aluminium. A gas pressure of 552 kPa was used to propel a 203.2 mm long striker bar. The flow stress computed was 450 MPa at a strain rate of 860 s^{-1}.

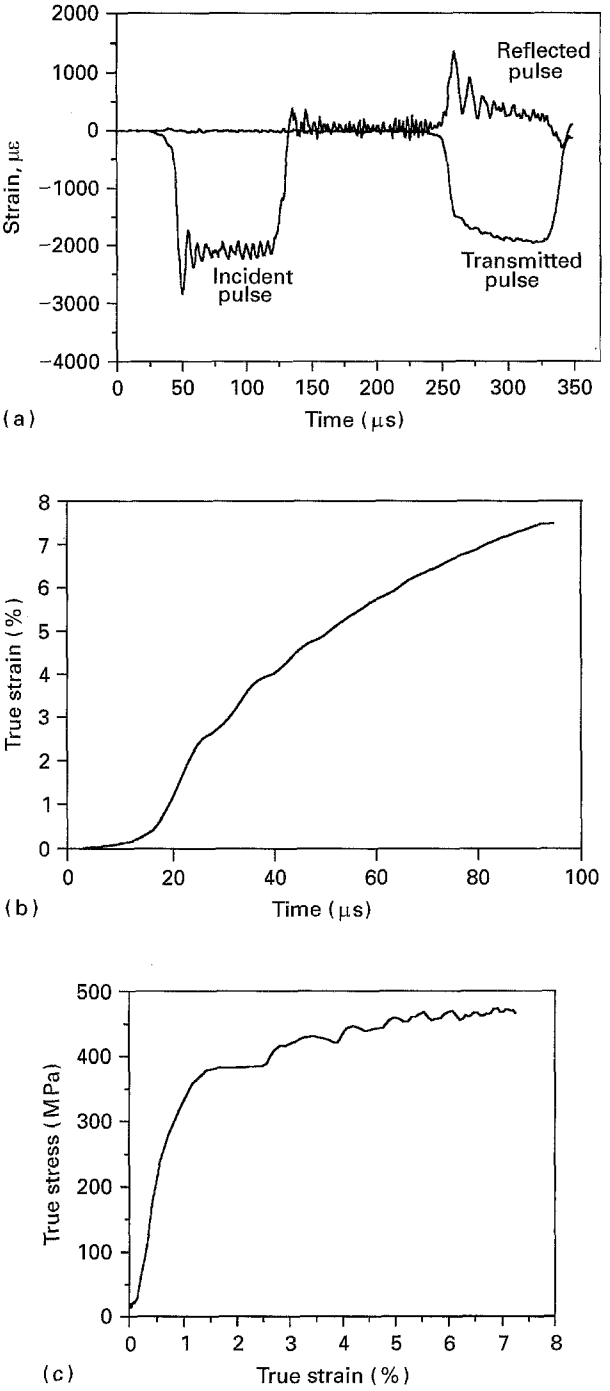

Figure 3 (a) Typical pulse profiles (raw data) obtained from the strain gauge data. (b) Typical true strain versus time curve obtained by integrating the reflected pulse of the SHPB pulse profiles. (c) Typical true stress versus true strain curve obtained from the SHPB data analysis.

4. Materials

4.1. SiC-reinforced composites

The silicon carbide-reinforced materials studied were SXA 2009 (S, silicon carbide; X, reinforced; A, aluminium) composites supplied by the Advanced Composite Material Corporation in Greer, SC. Two types of SiC-reinforced aluminium were tested. One composite was commercial 2009 aluminium reinforced with about 15% volume fraction SiC particles (SiC/Al-P). The second material was 2009 aluminium reinforced with about 15% volume fraction of SiC whiskers (SiC/Al-W). The materials were fabricated by an extrusion process and were supplied in 12.7 mm thick plate form.

The mechanical properties of both materials are tabulated in Table I. It was clear that the SiC/Al-P material was nearly isotropic and the SiC/Al-W material was highly anisotropic. It made no difference in the properties and response, whether the reinforcement was in the axial or transverse direction with respect to the axis of the compression specimen, in the case of particle-reinforced material. The mechanical properties also revealed that the reinforcing phase resulted in an increase in the elastic modulus, yield strength and ultimate strength compared to the properties of the matrix material.

The particle size varied from 0.5–4.0 μm while the whisker size varied from 0.5–15.0 μm in length with a diameter of 0.5 μm. The distribution of the reinforcing phase was also found to be non-uniform.

4.2. Fibre FP-reinforced composite

FP/Al is Fibre FP reinforced aluminium composite. The material is fabricated and supplied by DuPont. Fibre FP is a continuous polycrystalline alumina fibre and is prepared in the form of continuous yarn containing a nominal 200 filaments. Fibre FP is a ceramic fibre made of > 99% pure α-alumina. It has excellent chemical resistance and has higher modulus and temperature capability than ceramic fibres containing silica. The continuous fibre is easy to handle and can be oriented in desired directions. FP/Al is prepared by molten metal infiltration process. The volume fraction of the fibre in the composite is about 50%.

The FP/Al considered was a unidirectional composite and its mechanical properties are given in Table II.

It is evident from the properties that the composite will behave in a highly anisotropic manner. The tensile strength of the composite in the transverse direction is about a third of the strength in the axial direction. The compressive strength in the axial direction is about six times the tensile axial strength, fifteen times the transverse axial strength and about ten times the transverse compressive strength.

TABLE I Mechanical properties of SXA 2009 composites (as-received)

Material	Young's modulus (GPa)	0.2% offset yield stress (MPa)	Ultimate stress (MPa)
SiC/Al-P (axial)	93.2	228	410
SiC/Al-P (transverse)	84.9	228	399
SiC/Al-W (axial)	104	255	498
SiC/Al-W (transverse)	85.6	235	389

TABLE II Mechanical properties of FP/Al uni-directional composite

Direcion	Tensile strength (MPa)	Compressive strength (MPa)	Young's modulus (GPa)
Axial	551.6	3102.6	213.7
Transverse	189.6	362.0	144.8

TABLE III Macroscopic behaviour of different composites

Material	Striker bar (mm)	Gas pressure (kPa)	Maximum true strain (%)	Strain rate (s^{-1})	Flow stress (MPa)
SiC/Al-P	203.2	552	7	860	450
SiC/Al-P	101.6	690	13	3180	500
SiC/Al-W (axial)	203.2	552	2.8	345	500
SiC/Al-W (axial)	101.6	690	7	1715	720
SiC/Al-W (axial)	101.6	552	5.25	1285	700
SiC/Al-W (trans)	203.2	552	6.5	795	450
SiC/Al-W (trans)	101.6	690	13	3180	530
FP/Al (trans)	203.2	552	16	1960	270
FP/Al (trans)	101.6	414	13	3180	280

5. Results

Experiments were conducted on silicon carbide particle-reinforced aluminium (SiC/Al-P), silicon carbide whisker-reinforced aluminium (SiC/Al-W) and aluminium reinforced with continuous Fibre FP (FP/Al). All three materials were tested such that the compression specimen axes were taken both parallel and normal to the material extrusion direction. When the reinforcement was in the direction parallel to the extrusion direction, it was referred to as the "axial" direction. When the reinforcement was in the direction normal to the extrusion direction, it was referred to as the "transverse" direction. The specimens were also referred to as axial and transverse specimens.

The experimental results of all the composites tested are given in Table III.

6. Discussion

6.1. SiC/Al-P

In the case of SiC/Al particle-reinforced composite, it was observed that the values of flow stress in both cases were considerably higher than the yield stress of the material which is 228 MPa. The ultimate tensile strength of the material is 410 MPa. The flow stress values exceeded this value by 9.8% in the first case at a strain rate of 860 s^{-1}. In the second case the flow stress value exceeded the ultimate stress by 22% at a strain rate of 3180 s^{-1}. The value of flow stress was seen to increase with an increase in the strain rate of the experiment.

It was observed that there was strain hardening of the material. There was a non-uniform radial expansion due to slight anisotropy introduced by the reinforcing phase. The specimen cross section was elliptical after deformation with the major axis being 1.5% greater than the minor axis.

Fig. 4 shows the microstructure of the SiC/Al-P composite after deformation. Micro-cracks were observed at several locations on the specimen surface.

6.2. SiC/Al-W

Similar responses were observed in SiC/Al whisker-reinforced composites in both axial and transverse orientations of the reinforcing phase. The flow stress in the axial specimens was 500, 720 and 700 MPa at strain rates of 345, 1715 and 1285 s^{-1}, respectively. These values are 96.1%, 182.4% and 174.5% higher compared to the static tensile yield stress for this material which is 255 MPa. These values are 0.4%, 44.6% and 40.6% higher than even the ultimate tensile strength which is 498 MPa. In the case of transverse specimens the flow stress was 450 and 530 MPa at strain rates of 795 and 3180 s^{-1}, respectively. These flow stress values are 91.5% and 125.5% greater than the static tensile yield and 15.7% and 36.3% greater

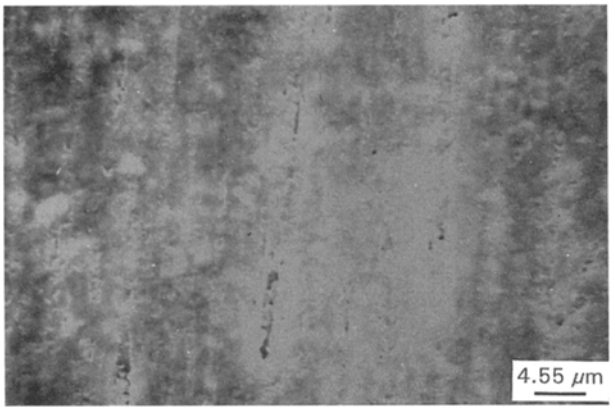

Figure 4 Scanning electron micrograph of the deformed SiC/Al particle-reinforced material showing several microcracks.

than the ultimate stress values in this orientation. In both the axial and transverse orientations of the specimen, ellipticity was observed in the specimens after deformation. In the case of axially oriented specimens the major axis exceeded the minor axis by 1.6% and in the transverse case the difference between the axes was 3.8%.

The high values of the dynamic flow stress in these experiments are clearly due to the strain-rate effect. The higher the strain rate of the experiment the greater was the flow stress value compared to the static yield or ultimate stress. One reason why the dynamic values are higher than the static values is due to the higher energy required to move dislocations that become piled up at grain boundaries. As the strain rate is increased, the faster the dislocation motion becomes, with no time available for energy redistribution within the material. Also, more energy will be required to move dislocations over the reinforcing phase.

In silicon carbide particle- and whisker-reinforced composites, matrix microcracking was prevalent. This suggests that failure in the material stems from around the hard reinforcing phase where the matrix starts to separate. Matrix separation occurs due to the tensile radial forces acting on the matrix/reinforcement interface. In comparison to Al 6061, the flow-stress levels in these materials are over twice as much. The static tensile strength of SiC/Al-P is 100 MPa more than that of Al 6061-T651. The average flow stress at similar strain rates, though, is higher by about 200 MPa. Similar increases were observed in the SiC/Al-W composites when compared to Al 6061-T651. Therefore, it is believed that the reinforcing material plays a significant role in high strain-rate loading response of the composite.

Fig. 5a and b show the microstructure of undeformed and deformed SiC/Al-W specimens. The microstructure of the deformed specimen revealed several micro-cracks (forming a network in several locations as in figure shown) in the matrix material.

Fig. 6a shows the SiC/Al-W transverse specimen before and after deformation. It was observed that the transverse specimen exhibited much more anisotropy than the axial specimen, as expected. There was no barrelling of the specimen.

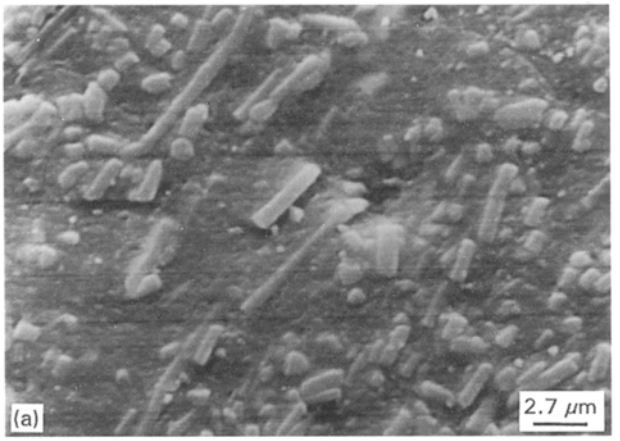

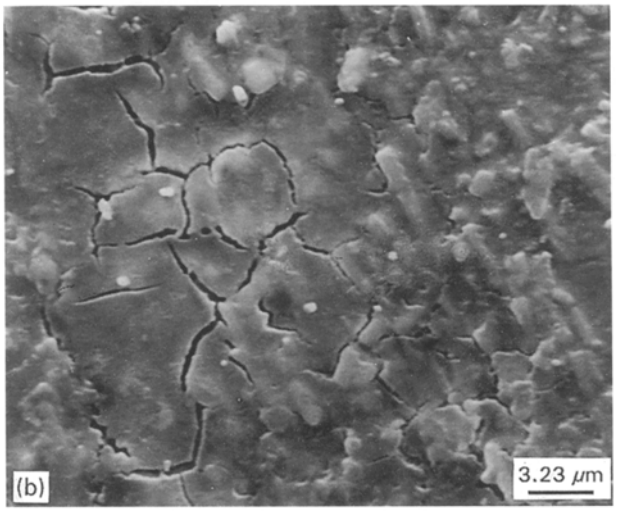

Figure 5 Scanning electron micrographs of (a) the undeformed Sic/Al whisker-reinforced material in the transverse direction, and (b) the deformed SiC/Al whisker-reinforced material in the transverse direction showing network microcracking.

6.3. FP/Al (transverse)

Fig. 6b illustrates the deformed and undeformed FP/Al transverse specimen in striking comparison to Fig. 6a. The degree of anisotropy is much higher in FP/Al transverse specimen than SiC/Al-W transverse specimen. There are two reasons for this. First, the volume fraction of the reinforcing phase is 50% in FP/Al compared to 15% in SiC/Al-W. Secondly, the reinforcing phase in the former is continuous and has a higher axial tensile modulus.

In FP/Al transverse specimens the flow stress computed was 270 and 280 MPa at strain rates of 1960 and 3180 s^{-1}. The strain achieved in the two cases was very high, being 16% in the first test case and 13% in the next. It was interesting to notice that the flow stress was lower than the static compressive strength, which is 362 MPa. It is this anomaly that lead to a closer observation of the mechanisms involved in the dynamic compressive response of transverse FP/Al specimens.

Fig. 7 is an optical micrograph of FP/Al axial specimen. It can be seen that the fibres form many clusters. Fig. 8a shows a scanning electron micrograph of the undeformed axial specimen microstructure. A good fibre/matrix interface is apparent. The specimen was

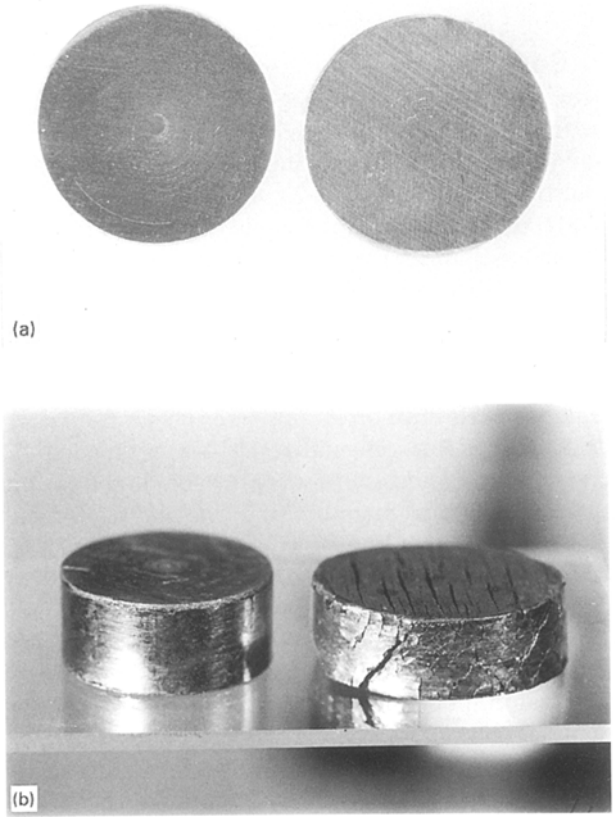

Figure 6 (a) SiC/Al-W (transverse) specimen before (left) and after (right) deformation. Note anisotropic radial expansion. (b) FP/Al (transverse) specimen before (left) and after (right) deformation. Again, note the high degree of anisotropic expansion.

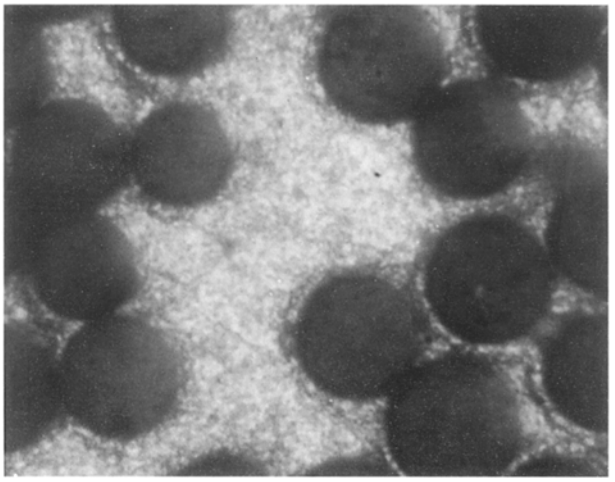

Figure 7 Optical micrograph of the undeformed FP/Al (axial) specimen showing clustering of fibres. Bright-field illumination.

compressed and the microstructure studied. Fig. 8b shows the deformed microstructure. The matrix can be seen to separate from the fibre.

Fig. 9 shows the scanning electron micrograph of the deformed FP/Al transverse specimen. There was excessive fragmentation and buckling of the fibres. The matrix separated from the fibres almost everywhere.

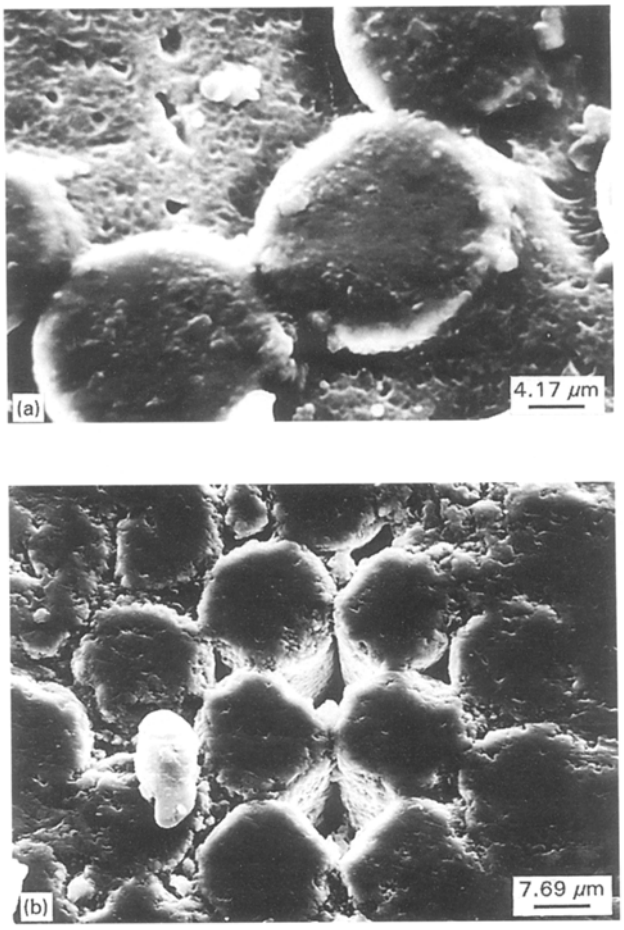

Figure 8 (a) Scanning electron micrograph of the undeformed FP/Al (Axial) specimen revealing a good fibre/matrix interface. (b) Deformed microstructure of the FP/Al (axial) specimen on SEM. Note fragmentation and separation of the matrix from the fibres.

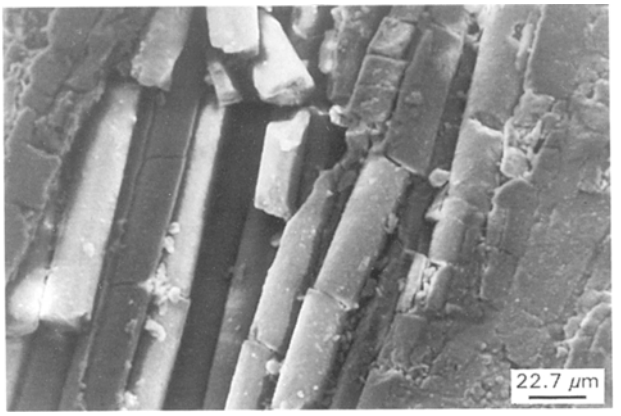

Figure 9 Deformed microstructure of the FP/Al (transverse) specimen on SEM. Note buckling, fragmentation and separation of fibres.

A close look at the macroscopic deformation of the transverse specimen not only revealed the high degree of anisotropy (with the major axis being 17% greater than the minor axis) but also the mode of failure, which was predominantly shear. Fig. 10 clearly illustrates this phenomenon. The specimens disintegrated in both the test cases and the lines of slip were at 45° angles, a clear indication of shear mode failure. It is proposed that the high volume fraction of fibres leads to initial compression of the various layers of fibres.

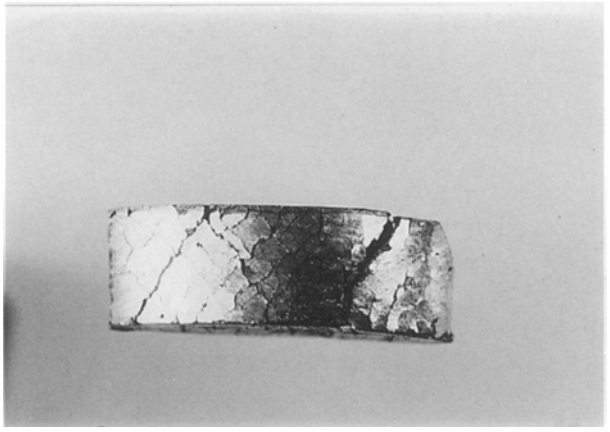

Figure 10 Side view of the FP/Al (tranverse) specimen after deformation. Note shearing.

Then, the impinging of very hard fibres on each other leads to slipping. The matrix separates from the fibre and the crack is rapidly propagated in shear mode leading to catastrophic failure. Microstructural observation also reveals that the fibres very close to each other break and buckle in phase, while the fibres separated by a relatively large amount of matrix, buckle out of phase. Buckling takes place due to the fact that the fibres resist the expansion of the matrix material along their length but pose relatively little resistance to the expansion in the direction perpendicular to their length. This is observed macroscopically as ovality of the deformed specimen. The low values of flow stress observed are, in fact, to a large extent due to damage propagation rather than pure compression.

6.4. FP/Al (axial)

There were several experiments conducted on FP/Al axial specimens. None of the experiments resulted in any appreciable strain in the specimens. The stress–strain plots could not be plotted due to the lack of appreciable reflected pulse in all the cases. The material is highly resistant to compressive loading as evident from Table II. The stress in the specimen should be in excess of 3000 MPa in order to be able to deform the FP/Al axial specimens plastically. This magnitude of stress was unattainable with the present apparatus. The yield stress of the bars was 2675 MPa and it was a necessary criterion that the bars remain perfectly elastic throughout the duration of the test. Also, the desired stress levels to deform the axial specimens were unattainable owing to the limitation of the pressure that can be built up in the gas chamber of the gas gun apparatus.

However, the impacted specimens were observed under the scanning electron microscope. Fig. 8b clearly shows that the matrix/fibre interface debonds. The large volume fraction of the reinforcing fibre FP phase takes the load and prevents the compression of the specimen. A cut section of the impacted specimen, when observed under the SEM revealed that the fibres began to break. It is intuitively predicted that the fibres would eventually break and lead to brittle mode failure of the specimen under extremely large loads.

7. Conclusion

The SHPB technique was used to study metal matrix composites, such as silicon carbide particle- and whisker-reinforced aluminium and Fibre FP-reinforced aluminium.

Macroscopic and microscopic characterization of the materials' response to high strain-rate loading was attempted. The macroscopic observations, such as increase in flow stress with the increase in strain rate, the anisotropy introduced due to the reinforcing phase, etc., were studied in conjunction with detailed metallography performed on the specimens before and after deformation. Experimental results show that microcracking within the grains was prevalent in the silicon carbide-reinforced materials and that the reinforcing phase plays a significant role in the macroscopic flow behaviour of these composites. In the case of FP/Al transverse specimens, results show that the material's dynamic flow stress values were considerably lower than the static compressive strength of the material. The failure mode observed in this orientation of the material was predominantly shear.

The applicability of the SHPB technique to high-strength materials, especially composites such as FP/Al in the axial configuration, is limited by the stress levels achievable by the apparatus. The FP/Al axial specimens were well within their elastic limits in all the tests conducted. However, it was shown that the SHPB technique could be successfully applied to characterize composite materials provided the materials' yield stresses are achievable with the apparatus.

Acknowledgements

The partial support of the National Science Foundation under grant MSS 9101514 is greatly acknowledged. The authors thank County Heat Treat, MA, for heat treating the pressure bars.

References

1. J. HOPKINSON, "Original papers by J. Hopkinson", Vol. 11, (Cambridge University Press, 1901) pp. 316–24.
2. B. HOPKINSON, *Proc. R. Soc. Lond. A* **74** (1905) 498.
3. *Idem, Phil. Trans. R. Soc. Lond. A* **213** (1914) 437.
4. H. KOLSKY, *Phil. Trans. R. Soc. Lond. B* **62** (1949) 676.
5. J. HARDING, E. O. WOOD and J. D. CAMPBELL, *J. Mech. Eng. Sci.* **2** (1960) 88.
6. U. S. LINDHOLM and L. M. YEAKLEY, *Exp. Mech.* **8** (1968) 1.
7. F. E. HAUSER, J. A. SIMMONS and J. E. DORN, in "Response of Metals to High Velocity Deformation, Metallurgical Society Conference", Vol. 9, edited by P. G. Shewmon and V. F. Zackay (Interscience, New York, 1961) p. 63.
8. W. E. BAKER and C. H. YEW, *J. Appl. Mech.* **33** (1966) 917.
9. J. L. CHIDDISTER and L. E. MALVERN, *Exp. Mech.* **3** (1963) 81.
10. U. S. LINDHOLM, *Mech. Phys. Solids* **12** (1964) 317.
11. E. D. H. DAVIES and S. C. HUNTER, *ibid.* **11** (1963) 155.

12. P. S. FOLLANSBEE, "Mechanical Testing, Metals Handbook", 9th Edn, Vol. 8 (ASM, Metals Park, OH, 1985) pp. 198–203.
13. S. NEMAT-NASSER, J. B. ISAACS and J. E. STARRETT, *Proc. R. Soc. Lond. A* **435** (1991) 371.
14. G. RAVICHANDRAN and W. CHEN, in "Experiments in Micromechanics of Failure Resistant Materials, AMD Vol. 130, edited by K. S. Kim (ASME, 1991) pp. 85–90
15. M. DA SILVA, and K. T. RAMESH, *ibid.*, pp. 105–18.
16. S. I. HONG, G. T. GRAY III and J. J. LEWANDOWSKI, *Acta Metall. Mater.* **41** (1993) 2337.

Received 12 October 1994
and accepted 28 April 1995